Radiation Hydrodynamics of Line-Driven Winds

Stan Owocki

Bartol Research Institute, Department of Physics and Astronomy
University of Delaware, Newark, DE 19716 USA

Abstract. Dimtri Mihalas' textbooks in the 70's and 80's on *Stellar Atmospheres* and *Foundations of Radiation Hydrodynamics* helped lay the early groundwork for understanding the moving atmospheres and winds of massive, luminous stars. Indeed, the central role of the momentum of stellar radiation in driving the mass outflow makes such massive-star winds key prototypes for radiation hydodynamical processes. This paper reviews the dynamics of such radiative driving, building first upon the standard CAK model, and then discussing subtleties associated with the development and saturation of instabilities, and wind initiation near the sonic point base. An overall goal is to illuminate the rich physics of radiative driving and the challenges that lie ahead in developing dynamical models that can explain the broad scalings of mass loss rate and flow speed with stellar properties, as well as the often complex structure and variability observed in massive-star outflows.

Keywords: Stars: Mass Loss
PACS: Pacs 97.10.Me Stellar characteristics and properties: Mass loss and stellar winds

INTRODUCTION

Through his textbooks and numerous papers, Dimitri Mihalas helped lay the groundwork for *radiation hydrodynamics* as an active discipline within astrophysics. Many of the contributions to this conference in his honor have emphasized the common roles that radiation plays both as a diagnostic and as an energy source/sink for astrophysical fluids. But perhaps the most fundamental aspect of radiation hydrodynamics arises when the *momentum* of radiation plays the central role in the dynamical driving of an astrophysical flow. A key prototype for this lies in the strong stellar winds from hot, massive, luminous stars, which are driven by the scattering of the star's continuum radiation flux by line-transitions of metal ions.

The discussion here aims to summarize some basic physical concepts from the nearly 4 decades of research since line-driving was first proposed as the mechanism for hot-star winds [15]. I begin with a summary of the standard CAK/Sobolev [3, 38] formalism for spherical, steady-state models of such winds. I then review subsequent studies that emphasize how relaxation of the Sobolev approximation for localized line-transport is central to modeling both the strong, small-scale instability of line-driving, as well as the wind initiation near the transonic wind base. A subtle but important aspect of this is the strong, dynamical role of the *diffuse* component of line-scattered radiation, which is entirely ignored in the standard CAK/Sobolev approach, but which can be approximately accounted for through *nonlocal, integral* forms for the escape probability.

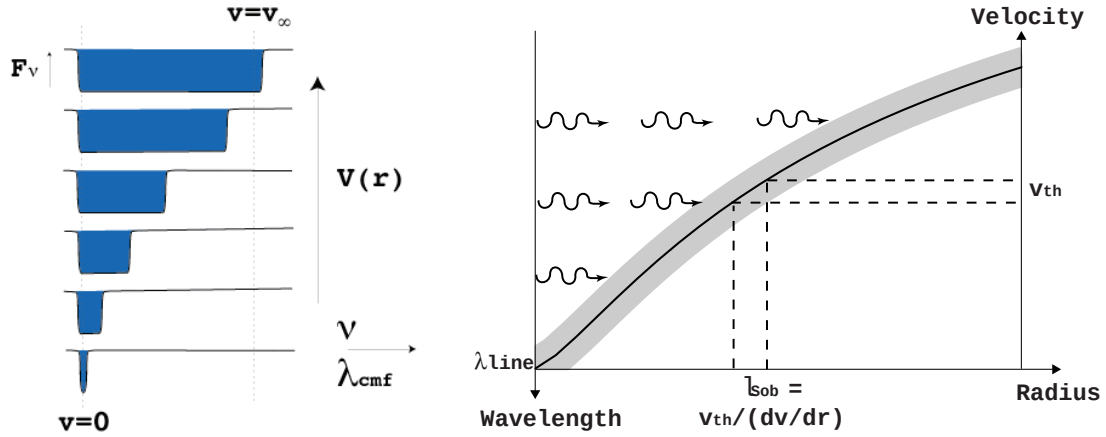

FIGURE 1. Two perspectives for the Doppler-shifted line-resonance in an accelerating flow. Right: Photons with a wavelength just shortward of a line propagate freely from the stellar surface up to a layer where the wind outflow Doppler shifts the line into a resonance over a narrow width (represented here by the shading) equal to the Sobolev length, set by the ratio of thermal speed to velocity gradient, $l_{Sob} \equiv v_{th}/(dv/dr)$. Left: Seen from successively larger radii within the accelerating wind, the Doppler-shift sweeps out an increasingly broadened line absorption trough in the stellar spectrum.

THE CAK/SOBOLEV MODEL FOR STEADY WINDS

Consider a steady-state stellar wind outflow in which the radiative acceleration g_{rad} overcomes the local gravity GM_*/r^2 at radius r to drive a net acceleration $v(dv/dr)$ in the radial flow speed $v(r)$. Since overcoming gravity is key, it is convenient to define a dimensionless equation of motion that scales all accelerations by gravity,

$$(1 - w_s/w)\, w' = -1 + \Gamma_{rad}\,, \tag{1}$$

where $\Gamma_{rad} \equiv g_{rad}\, r^2/GM_*$, $w \equiv v^2/v_{esc}^2$, and $w' \equiv dw/dx$, with $x \equiv 1 - R_*/r$ and $v_{esc} \equiv \sqrt{2GM_*/R_*}$ the escape speed from the stellar surface radius R_*. Eqn. (1) neglects gas pressure terms on the right side, since for isothermal sound speed a these are of order $w_s \equiv (a/v_{esc})^2 \approx 0.001$ compared to competing terms needed to drive the wind.

For pure electron scattering opacity κ_e, the scaled radiative acceleration is just the usual Eddington parameter [6],

$$\Gamma_e \equiv \frac{\kappa_e L_*}{4\pi G M_* c} = 2 \times 10^{-5}\, \frac{L_*/L_\odot}{M_*/M_\odot}\,. \tag{2}$$

Because typically $L_* \sim M_*^{3-3.5}$, stars with $M_* > 10 M_\odot$ have $\Gamma_e > 10^{-3}$, with the Eddington limit $\Gamma_e \to 1$ perhaps even being central to setting a stellar upper mass limit of $M_* \leq 150 M_\odot$ [9]. Eruptive mass loss from luminous blue variable (LBV) stars like η Carinae might in fact be continuum-driven during episodes of super-Eddington luminosity [4, 22, 28].

But the resonant nature of line (bound-bound) scattering from metal ions leads to an opacity that is inherently much stronger than from free electrons. For example, in the

somewhat idealized, *optically thin* limit that all the line opacity could be illuminated with a flat, unattenuated continuum spectrum with the full stellar luminosity, the total line-force would exceed the free-electron force by a huge factor, of order $\overline{Q} \approx 2000$ [11]. This implies line-driven winds can be initiated in even moderately massive stars with $\Gamma_e > 5 \times 10^{-4}$, while for more massive stars with $\Gamma_e \approx 1/2$, the net outward line acceleration in principle could be as high as $\Gamma_{thin} \approx \overline{Q}\Gamma_e \approx 1000$ times the acceleration of gravity!

In practice, self-absorption within strong lines limits the acceleration, with the mass loss rate $\dot{M}$ set at the level for which the line driving is just sufficient to overcome gravity. Indeed line-saturation keeps the dense, nearly static layers of the atmosphere gravitationally bound. But as illustrated by figure 1, within the accelerating wind, the Doppler shift of the line-resonance out of the absorption shadow of underlying material exposes the line opacity to a less attenuated flux. This effectively desaturates the lines by limiting the resonance to a layer with width set by the Sobolev length, $l_{Sob} = v_{th}/(dv/dr)$, and with optical depth proportional to $t \equiv \kappa_e \rho c/(dv/dr) = \Gamma_e \dot{M} c^2/L_* w'$.

For the CAK line-ensemble with a power-law number distribution in line-strength, the cumulative force is reduced by a factor $1/(\overline{Q}t)^\alpha$ from the optically thin value,

$$\Gamma_{CAK} = \frac{\overline{Q}\Gamma_e}{(1-\alpha)(\overline{Q}t)^\alpha} = \Gamma_e k t^{-\alpha} = C(w')^\alpha \,, \tag{3}$$

where the second equality defines the CAK "force muliplier" $kt^{-\alpha}$, with[1] $k \equiv \overline{Q}^{1-\alpha}/(1-\alpha)$. The last equality relates the line-force to the flow acceleration, with

$$C \equiv \frac{1}{1-\alpha}\left[\frac{L_*}{\dot{M}c^2}\right]^\alpha \left[\overline{Q}\Gamma_e\right]^{1-\alpha} . \tag{4}$$

Note that, for fixed sets of parameters for the star (L_*, M_*, Γ_e) and line-opacity (α, $\overline{Q}$), this constant scales with the mass loss rate as $C \propto 1/\dot{M}^\alpha$.

Neglecting the small sound-speed term $w_s \approx 0.001 \ll 1$, application of eqn. (3) into (1) gives the CAK equation of motion,

$$F = w' + 1 - \Gamma_e - C(w')^\alpha = 0 \,. \tag{5}$$

For small $\dot{M}$ (large C), there are two solutions, while for large $\dot{M}$ (small C), there are no solutions. The CAK critical solution corresponds to a *maximal* mass loss rate, defined by $\partial F/\partial w' = 0$, for which the $C(w')^\alpha$ is tangent to the line $1 - \Gamma_e + w'$ at a critical acceleration $w'_c = (1-\Gamma_e)\alpha/(1-\alpha)$. Since the scaled equation of motion (5) has no explicit spatial dependence, this critical acceleration applies throughout the wind, and

---

[1] Here we use a slight variation of the standard CAK notation in which the artificial dependence on a fiducial ion thermal speed is avoided by simply setting $v_{th} = c$. Backconversion to CAK notation is achieved by multiplying t by v_{th}/c and k by $(v_{th}/c)^\alpha$. The line normalization $\overline{Q}$ offers the advantages of being a dimensionless measure of line-opacity that is independent of the assumed ion thermal speed, with a nearly constant characteristic value of order $\overline{Q} \sim 10^3$ for a wide range of ionization conditions [11].

so can be trivially integrated to yield $w(x) = w_c' x$. In terms of dimensional quantities, this represents a specific case of the general "beta"-velocity-law,

$$v(r) = v_\infty \left(1 - \frac{R_*}{r}\right)^\beta , \tag{6}$$

where here $\beta = 1/2$, and the wind terminal speed $v_\infty = v_{esc}\sqrt{\alpha(1-\Gamma_e)/(1-\alpha)}$. Similarly, the critical value C_c yields, through eqn. (4), the standard CAK scaling for the mass loss rate

$$\dot{M}_{CAK} = \frac{L_*}{c^2}\,\frac{\alpha}{1-\alpha}\left[\frac{\overline{Q}\Gamma_e}{1-\Gamma_e}\right]^{(1-\alpha)/\alpha} . \tag{7}$$

These CAK results strictly apply only under the idealized assumption that the stellar radiation is radially streaming from a point-source. If one takes into account the finite angular extent of the stellar disk, then near the stellar surface the radiative force is reduced by a factor $f_{d*} \approx 1/(1+\alpha)$, leading to a reduced mass loss rate [10, 30]

$$\dot{M}_{fd} = f_{d*}^{1/\alpha}\dot{M}_{CAK} = \frac{\dot{M}_{CAK}}{(1+\alpha)^{1/\alpha}} \approx \dot{M}_{CAK}/2 . \tag{8}$$

Away from the star, the correction factor increases back toward unity, which for the reduced base mass flux implies a stronger, more extended acceleration, giving a somewhat higher terminal speed, $v_\infty \approx 3v_{esc}$, and a flatter velocity law, approximated by replacing the exponent in eqn. (6) by $\beta \approx 0.8$.

The effect of a radial change in ionization can be approximately taken into account by correcting the CAK force (3) by a factor of the form $(n_e/W)^\delta$, where n_e is the electron density, $W \equiv 0.5(1-\sqrt{1-R_*/r})$ is the radiation "dilution factor", and the exponent has a typical value $\delta \approx 0.1$ [11]. This factor introduces an additional density dependence to that already implied by the optical depth factor $1/t^\alpha$ given in eqn. (3). Its overall effect can be roughly accounted with the simple substition $\alpha \rightarrow \alpha' \equiv \alpha - \delta$ in the power exponents of the CAK mass loss scaling law (7). The general tendency is to moderately increase $\dot{M}$, and accordingly to somewhat decrease the wind speed.

The above scalings also ignore the finite gas pressure associated with a small but non-zero sound-speed parameter w_s. Through a perturbation expansion of the equation of motion (1) in this small parameter, it possible to derive simple scalings for the fractional corrections to the mass loss rate and terminal speed [27],

$$\delta m_s \approx \frac{4\sqrt{1-\alpha}}{\alpha}\,\frac{a}{v_{esc}} \quad ; \quad \delta v_{\infty,s} \approx \frac{-\alpha\delta m_s}{2(1-\alpha)} \approx \frac{-2}{\sqrt{1-\alpha}}\,\frac{a}{v_{esc}} . \tag{9}$$

For a typical case with $\alpha \approx 2/3$ and $w_s = 0.001$, the net effect is to increase the mass loss rate and decrease the wind terminal speed, both by about 10%.

Finally, an important success of these CAK scaling laws is the theoretical rationale they provide for an empirically observed "Wind-Momentum-Luminosity" (WML) relation [12]. Combining the CAK mass-loss law (7) together with the scaling of the terminal

speed with the effective escape, we obtain a WML relation of the form,

$$\dot{M}v_\infty\sqrt{R_*} \sim L^{1/\alpha'}\overline{Q}^{1/\alpha'-1} \tag{10}$$

wherein we have neglected a residual dependence on $M(1-\Gamma_e)$ that is generally very weak for the usual c ase that α' is near $2/3$. Note that the direct dependence $\overline{Q} \sim Z$ provides the scaling of the WML with metalicity Z.

NON-SOBOLEV WIND INSTABILITY & INITIATION

The above CAK steady-state model depends crucially on the use of the Sobolev approximation to compute the local CAK line force (3). Analyses that relax this approximation show that the flow is subject to a strong, "line-deshadowing instability" (LDI) for velocity perturbations on a scale near and below the Sobolev length $l_{Sob} = v_{th}/(dv/dr)$ [15, 16, 25, 26, 23]. Moreover, the diffuse, scattered component of the line force, which in the Sobolev limit is nullified by the fore-aft symmetry of the Sobolev escape probability (see figure 2b), turns out to have important dynamics effects on both the instability and sonic-point initiation of the wind.

Linear Analysis of Line-Deshadowing Instability

For sinusoidal perturbations ($\sim e^{i(kr-wt)}$) with wavenumber k and frequency ω, the linearized momentum equation (ignoring the small gas pressure) relating the perturbations in velocity and radiative acceleration implies

$$\omega = i\frac{\delta g}{\delta v}\,, \tag{11}$$

which shows that unstable growth, with $\Im\omega > 0$, requires $\Re(\delta g/\delta v) > 0$. For a purely Sobolev model [1], the CAK scaling of the line-force (3) with velocity gradient v' implies $\delta g \sim \delta v' \sim ik\delta v$, giving a purely real ω, and thus a stable wave that propagates inward at phase speed,

$$\frac{\omega}{k} = -\frac{\partial g}{\partial v'} \equiv -U\,, \tag{12}$$

which is now known as the "Abbott speed". Abbott [1] showed this is comparable to the outward wind flow speed, and in fact exactly equals it at the CAK critical point.

As illustrated in figure 2a, instability arises from the deshadowing of the line by the extra Doppler shift from the velocity perturbation, giving $\delta g \sim \delta v$ and thus $\Im\omega > 0$. A general analysis [25] yields a "bridging law" encompassing both effects,

$$\frac{\delta g}{\delta v} \approx \Omega\frac{ik\Lambda}{1+ik\Lambda}\,, \tag{13}$$

where $\Omega \approx g_{cak}/v_{th}$ sets the instability growth rate, and the "bridging length" Λ is found to be of order the Sobolev length l_{sob}. In the long-wavelength limit $k\Lambda \ll 1$, we recover

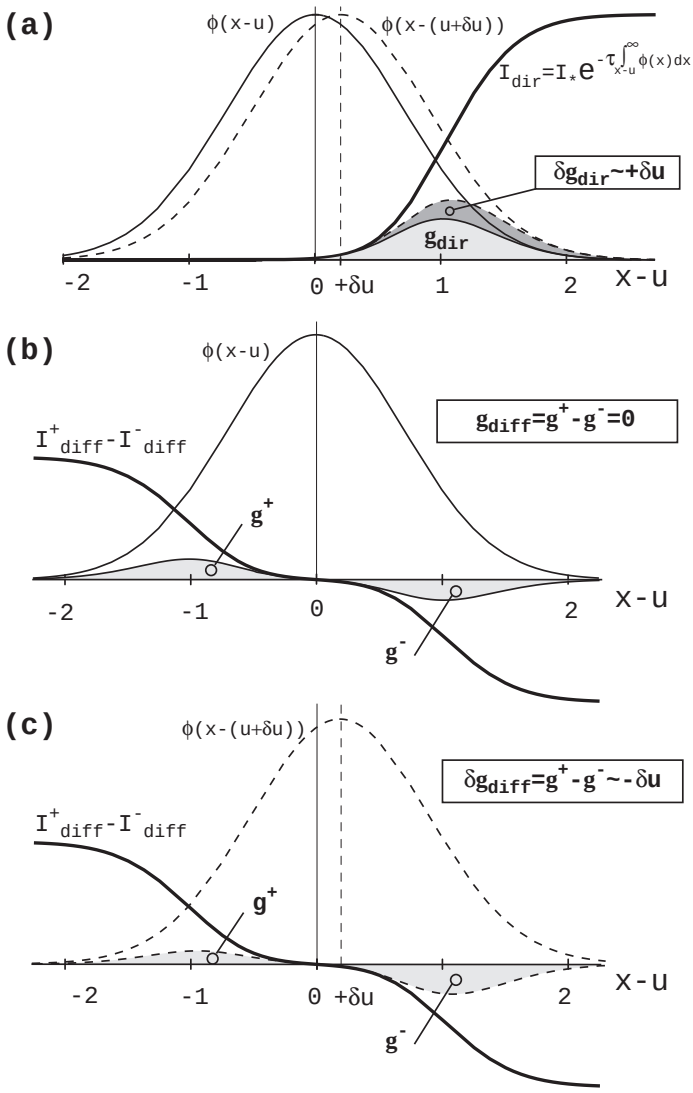

FIGURE 2. (a) The line profile ϕ and direct intensity plotted vs. comoving frame frequency $x-u = x - v/v_{th}$, with the light shaded overlap area proportional to the net direct line-force g_{dir}. The dashed profile shows the effect of the Doppler shift from a perturbed velocity δv, with the resulting extra area in the overlap with the blue-edge intensity giving a perturbed line-force δg that scales in proportion to this perturbed velocity $\delta u = \delta v/v_{th}$. (b) The comoving-frequency variation of the forward (+) and backward (-) streaming parts of the diffuse, scattered radiation, illustrating the cancelling of the overlap with the line profile that causes the net diffuse force to nearly vanish in a smooth, supersonic outflow. (c) However, because of the Doppler shift from the perturbed velocity, the dashed profile now has a stronger interaction with the backward streaming diffuse radiation. This results in a diffuse-line-drag force that scales with the negative of the perturbed velocity, and so tends to counter the instability of the direct line-force in part a.

the stable, Abbott-wave scalings of the Sobolev approximation, $\delta g/\delta v \approx ik\Omega\Lambda = ikU$; while in the short-wavelength limit $k\Lambda \gg 1$, we obtain the instability scaling $\delta g \approx \Omega \delta v$. The instability growth rate is very large, about the flow rate through the Sobolev length, $\Omega \approx v/l_{Sob}$. Since this is a large factor v/v_{th} bigger than the typical wind expansion rate

$dv/dr \approx v/R_*$, a small perturbation at the wind base would, within this lineary theory, be amplified by an enormous factor, of order $e^{v/v_{th}} \approx e^{100}$!

Numerical Simulations of Instability-Generated Wind Structure

Numerical simulations of the nonlinear evolution require a non-Sobolev line-force computation on a spatial grid that spans the full wind expansion over several R_*, yet resolves the unstable structure at small scales near and below the Sobolev length. The first tractable approach [20] focussed on the *absorption* of the *direct* radiation from the stellar core, accounting now for the attenuation from intervening material by carrying out a *nonlocal integral* for the frequency-dependent radial optical depth,

$$t(x,r) \equiv \int_{R_*}^{r} dr' \kappa_e \rho(r') \phi \left[x - v(r')/v_{th} \right] , \tag{14}$$

where ϕ is the line-profile function, and x is the observer-frame frequency from line-center in units of the line thermal width. The corresponding nonlocal form for the CAK line-ensemble force from this direct stellar radiation is

$$\Gamma_{dir}(r) = \Gamma_e \overline{Q}^{1-\alpha} \int_{-\infty}^{\infty} dx \, \frac{\phi \left(x - v(r)/v_{th} \right)}{t(x,r)^{\alpha}} . \tag{15}$$

In the Sobolev approximation, $t(x,r) \approx \Phi(x - v/v_{th})t$ (where $\Phi(x) \equiv \int_x^{\infty} \phi(x')\, dx'$), this recovers the CAK form (3). But for perturbations on a spatial scale near and below the Sobolev length, its variation also scales in proportion to the perturbed velocity, leading to unstable amplification. Simulations show that because of inward nature of wave propagation implies an anti-correlation between velocity and density variation, the nonlinear growth leads to high-speed rarefactions that steepen into strong *reverse* shocks and compress material into dense clumps (or shells in these 1D models) [20].

The assumption of pure-absorption was criticized by Lucy [13], who pointed out that the interaction of a velocity perturbation with the background, *diffuse* radiation from line-scattering results in a *line-drag* effect that reduces, and potentially could even eliminate, the instability associated with the direct radiation from the underlying star. The basic effect is illustrated in figure 2. Panel b shows how the fore-aft ($\pm$) symmetry of the diffuse radiation leads to cancellation of the g_+ and g_- force components from the forward and backward streams, as computed from a line-profile with frequency centered on the local comoving mean flow. In contrast, panel c shows that the Doppler shift associated with the velocity perturbation δv breaks this symmetry, and leads to stronger forces from the component opposing the perturbation.

Full linear stability analyses accounting for scattering effects [26, 23] show the fraction of the direct instability that is canceled by the line-drag of the perturbed diffuse force depends on the ratio of the scattering source function S to core intensity I_c,

$$s = \frac{r^2}{R_*^2} \frac{2S}{I_c} \approx \frac{1}{1+\mu_*} \quad ; \quad \mu_* \equiv \sqrt{1 - R_*^2/r^2} , \tag{16}$$

where the latter approximation applies for the optically thin form $2S/I_c = 1-\mu_*$. The net instability growth rate thus becomes

$$\Omega(r) \approx \frac{g_{cak}}{v_{th}} \frac{\mu_*(r)}{1+\mu_*(r)} \,. \tag{17}$$

This vanishes near the stellar surface, where $\mu_* = 0$, but it approaches half the pure-absorption rate far from the star, where $\mu_* \to 1$. This implies that the outer wind is still very unstable, with cumulative growth of ca. $v_\infty/2v_{th} \approx 50$ e-folds.

Most efforts to account for scattering line-drag in simulations of the nonlinear evolution of the instability have centered on a *Smooth Source Function* (SSF) approach [18, 7, 23, 24]. This assumes that averaging over frequency and angle makes the scattering source function relatively insensitive to flow structure, implying it can be pulled out of the integral in the formal solution for the diffuse intensity. Within a simple *two-stream* treatment of the line-transport, the net diffuse line-force then depends on the *difference* in the *nonlocal* escape probabilities $b_\pm$ associated with forward (+) vs. backward (-) *integrals* of the frequency-dependent line-optical-depth (14). For a CAK line-ensemble, the net diffuse force can be written in a form quite analogous to the direct component (15),

$$\Gamma_{diff}(r) = \frac{\Gamma_e \overline{Q}^{1-\alpha}}{2(1+\mu_*)} \left[b_-(r) - b_+(r) \right] \,, \tag{18}$$

with

$$b_\pm(r) \equiv \int_{-\infty}^{\infty} dx \frac{\phi(x - v(r)/v_{th})}{\left[t_\pm(\pm x, r) \right]^\alpha} \tag{19}$$

where[2] for t_- the integral bounds in (14) are now from r to the outer radius R_{max} [23, 19], and the overall normalization for Γ_{diff} assumes the optically thin source function from eqn. (16). In the Sobolev approximation, both the forward and backward integrals give the same form, viz. $t_\pm(\pm x, r) \approx \Phi[\pm(x - v/v_{th})]t$, leading to the net cancellation of the Sobolev diffuse force (figure 2b). But for perturbations on a spatial scale near and below the Sobolev length, the perturbed velocity breaks the forward/back symmetry (figure 2c), leading to perturbed diffuse force that now scales in proportion to the *negative* of the perturbed velocity, and thus giving the diffuse line-drag that reduces the net instability by the factors given in (16) and (17).

The left panel of figure 3 illustrates the results of a 1D SSF simulation, starting from an initial condition set by smooth, steady-state CAK/Sobolev model (dashed curves). Because of the line-drag stabilization of the driving near the star (eqn. 17), the wind base remains smooth and steady. But away from the stellar surface, the net strong instability leads to extensive structure in both velocity and density, roughly straddling the CAK steady-state. Because of the backstreaming component of the diffuse line-force causes

---

[2] To account for the nonradial radiation from a finite-angle star, in practice SSF models carry out the forward/back optical depth integrals along a ray with an impact parameter that is $R_\star/\sqrt{2}$ off the disk center. A similar application for the direct force (15) gives within a few percent the proper finite-disk correction to the CAK/Sobolev point-star line-force (3) in a smooth flow.

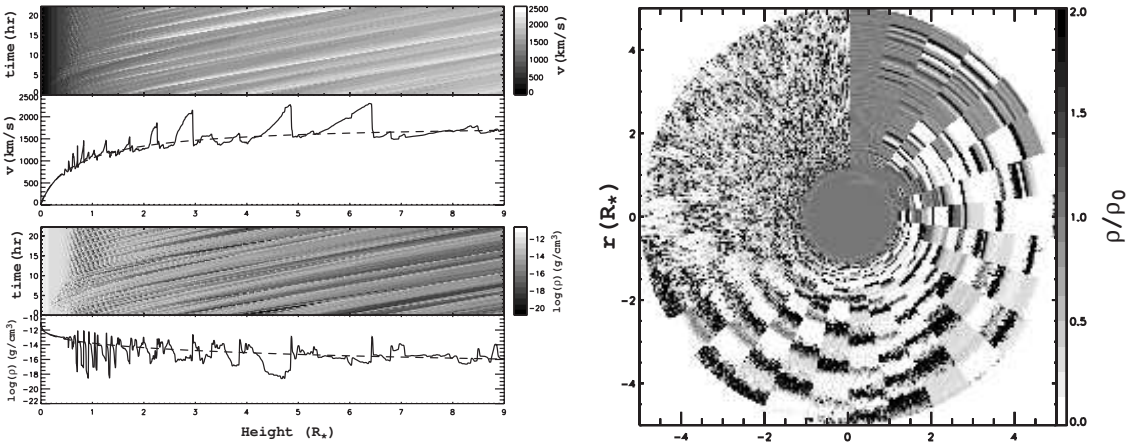

FIGURE 3. Left: Results of 1D Smooth-Source-Function (SSF) simulation of the line-deshadowing instability. The line plots show the spatial variation of velocity (upper) and density (lower) at a fixed, arbitrary time snapshot. The corresponding grey scales show both the time (vertical axis) and height (horizontal axis) evolution. The dashed curve shows the corresponding smooth, steady CAK model. Right: For 2DH+1DR SSF simulation, grayscale representation for the density variations rendered as a time sequence of 2-D wedges of the simulation model azimuthal range $\Delta\phi = 12^o$ stacked clockwise from the vertical in intervals of 4000 sec from the CAK initial condition.

any outer wind structure to induce small-amplitude fluctuations near the wind base, the wind structure, once initiated, is "self-excited", arising spontaneously without any explict perturbation from the stellar boundary.

In the outer wind, the velocity variations become highly nonlinear and nonmonotonic, with amplitudes approaching 1000 km/s, leading to formation of strong shocks. However, these high-velocity regions have very low density, and thus represent only very little material. As noted for the pure-absorption models, this anti-correlation between velocity and density arises because the unstable linear waves that lead to the structure have an *inward* propagation relative to the mean flow. For most of the wind mass, the dominant overall effect of the instability is to concentrate material into dense clumps, which can lead to substantial (factor 3-5) overestimates in the mass loss rate from diagnostics (e.g. radio or Balmer emission) that scale with the square of the density.

The presence of multiple, embedded strong shocks suggests a potential source for the soft X-ray emission observed from massive star winds; but the rarefied nature of the high-speed gas implies that this self-excited structure actually feeds very little material through the strong shocks needed to heat gas to X-ray emitting temperatures. To increase the level of X-ray emission, Feldmeier [8] introduced intrinsic perturbations at the wind base, assuming the underlying stellar photosphere has a turbulent spectrum of compressible sound waves characterized by abrupt phase shifts in velocity and density. These abrupt shifts seed wind variations that, when amplified by the line-deshadowing instabilty, now include substantial velocity variations among the dense clumps. As illustrated in figure 4, when these dense clumps collide, they induce regions of relatively dense, hot gas which produce localized bursts of X-ray emission. Averaged over time, these localized regions can collectively yield X-ray emission with a brightness and spectrum that is comparable to what is typically observed from such hot stars.

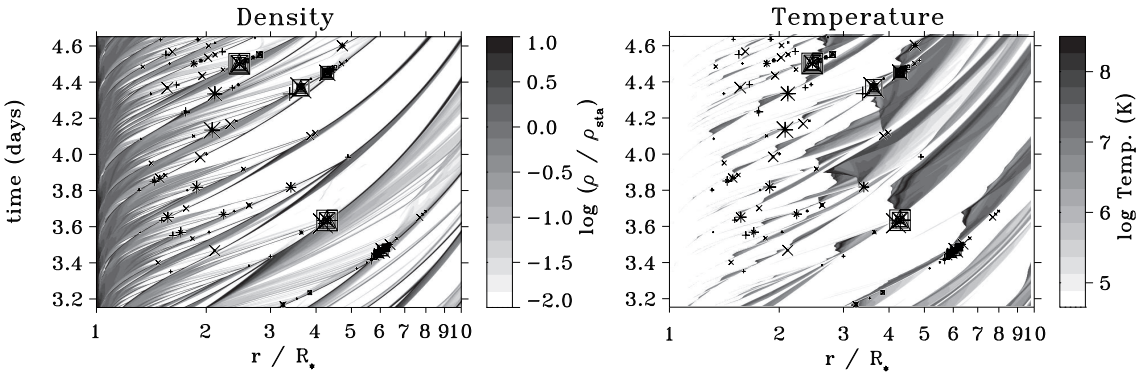

FIGURE 4. Greyscale rendition of the evolution of wind density and temperature, for time-dependent wind-instability models with structure formation triggered by photospheric perturbations. The boxed crosses identify localized region of clump-clump collision that lead to the hot, dense gas needed for a substantial level of soft X-rays emission.

Because of the computational expense of carrying out nonlocal optical depth integrations at each time step, such SSF instability simulations have generally been limited to just 1D. More realistically, various kinds of thin-shell instabilites [39] can be expected to break up the structure into a complex, multidimensional form. A first step to modelling both radial and lateral structure [5] is to use a restricted "2D-H+1D-R" approach, extending the hydrodynamical model to 2D in radius and azimuth, but still keeping the 1D-SSF radial integration for the inward/outward optical depth within each azimuthal zone. The right panel of figure 3 shows the resulting 2D density structure within a narrow (12^o) wedge, with the time evolution rendered clockwise at fixed time intervals of 4000 sec starting from the CAK initial condition at the top. The line-deshadowing instability is first manifest as strong radial velocity variations and associated density compressions that initially extend nearly coherently across the full azimuthal range of the computational wedge.

But as these initial "shell" structures are accelerated outward, they become progressively disrupted by Rayleigh-Taylor or thin-shell instabilities that operate in azimuth down to the grid scale $d\phi = 0.2^o$. Such a 2DR+1DH approach may well exaggerate the level of variation on small lateral scales. The lack of *lateral* integration needed to compute an azimuthal component of the diffuse line-force means that the model ignores a potentially strong net lateral line-drag that should strongly damp azimuthal velocity perturbations on scales below the lateral Sobolev length $l_0 \equiv r v_{th}/v_r$ [36]. Presuming that this would inhibit development of lateral instability at such scales, then any lateral breakup would be limited to a minimum lateral angular scale of $\Delta\phi_{min} \approx l_0/r = v_{th}/v_r \approx 0.01\,\mathrm{rad} \approx 0.5^o$. Further work is needed to address this issue through explicit incorporation of the lateral line-force and the associated line-drag effect.

Overall, both the 1D and 2D SSF simulations suggest that the LDI results naturally in strong, small-scale clumping, implying a significant (factor several) reduction in mass loss rates deduced from density-squared diagnostics. On the other hand, the small scale makes it unlikely individual clumps can become optically thick, and so lead to a signifcant wind "porosity" that would weaken *single*-density processes like bound-free

absorption of X-rays [21, 17]. Together these suggest the observed weak asymmetry of X-ray emission lines from massive stars may be mainly the result of a reduced mass loss rate, and not wind porosity.

Escape Integral Source Function Method and Wind Initiation

Finally, a full linear analysis of the effects of scattering on the line-deshadowing instability [26] shows that perturbations in the line source function can lead to unstable wavemodes that now have *outward* phase propagation. Since such outward wavemodes have a positive correlation between density and velocity, this raises the possibility that the nonlinear amplification of velocity perturbations might now lead to strong *forward* shocks; this could cause a much larger fraction of wind material to be heated to X-ray emitting temperatures, as needed to explain the observed X-ray emission [32].

These possibilities motivated development [23] of a new *Escape Integral Source Function* (EISF) that now re-uses the nonlocal escape probabilities $b_\pm$ defined in eqn. (19) to estimate the dynamical variation of the source function,

$$S(r) \approx I_c \, [1 - \mu_*(r)] \; \frac{b_+(r)}{b_+(r) + b_-(r)} \, . \tag{20}$$

Using this $S(r)$ within a formal solution for the diffuse intensity thus provides the basis for a computation of the diffuse line-force that accounts for both the line-drag and phase reversal effects [23].

Application in an EISF simulation code [24] indeed confirms that the initial linear onset of the wind instability is dominated by variations with a *positive* correlation between density and velocity. However, the self-shadowing of radiative driving from such denser, faster structures makes their growth *saturate* at a low amplitude, about the thermal speed v_{th}. Eventually, the wind structure thus again becomes dominated by the slower, but less-saturated growth of variations with the usual anti-correlation between velocity and density. Overall, the fully developed wind structure in EISF models thus turns out to be quite similar to the SSF case, with no apparent tendency to produce denser, forward shocks that might give stronger X-ray emission.

But perhaps the biggest surprise from these EISF simulations regards the subtle nature of the wind initiation near the sonic point base. Because the ion thermal speed v_{th} is only moderately smaller than the sound speed a, the Sobolev length $l_{Sob} = v_{th}/(dv/dr)$ near the sonic point becomes comparable to the characterize density/velocity scale length $H \approx v/(dv/dr)$, thus raising questions about the suitability of using the Sobolev-based CAK line-force to model the wind driving in this transonic region. The left panel of figure 5 plots the spatial variation of various line-force components within the transonic wind based of a CAK initial condition, for both SSF (upper) and EISF (lower) models with a typical thermal to sound speed ratio $v_{th}/a = 0.28$. Note first that in both models, the direct force lies well below the CAK/Sobolev force throughout the subsonic region; as first noted by Poe et al. [31], this gives non-Sobolev pure-absorption models a quite different character than the usual CAK/Sobolev solution.

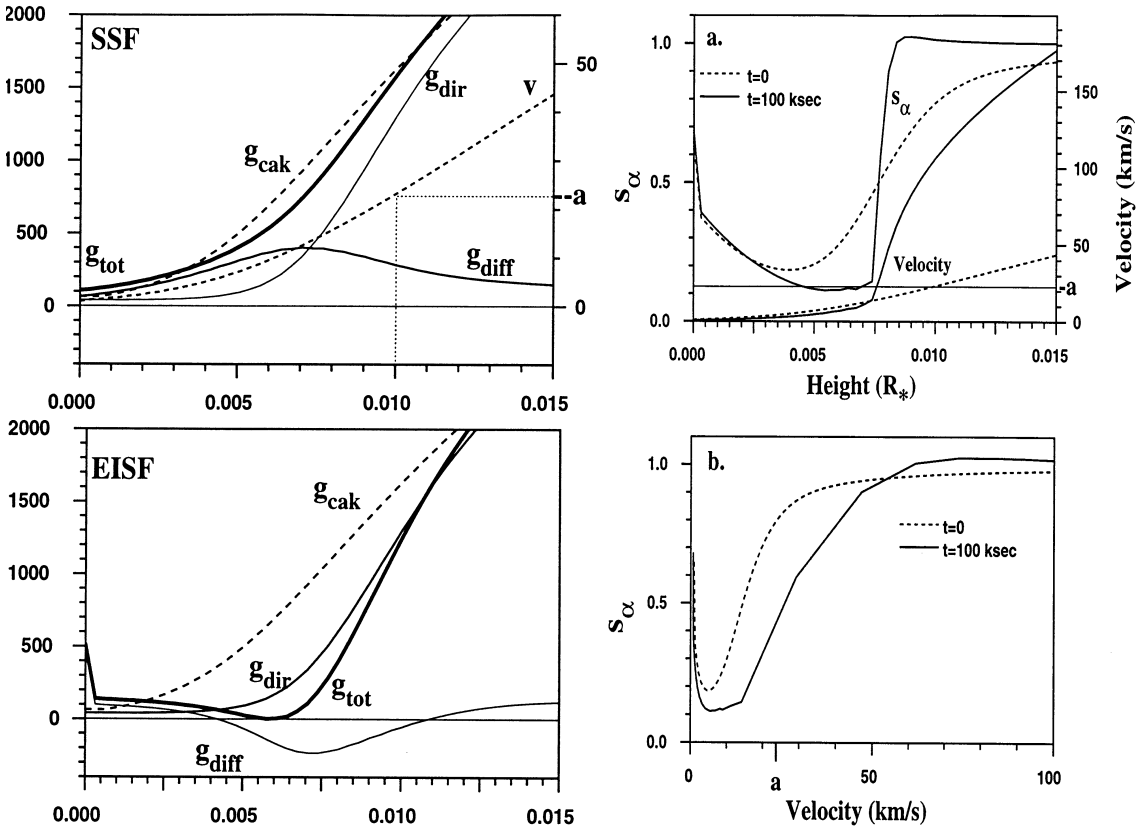

FIGURE 5. Left: Spatial variation of the velocity and various components of the line force near the transonic wind base for the SSF (top) and EISF (bottom) models, computed at the CAK initial condition. The location of the sonic point is indicated by dotted lines in the uppermost panel. Right: a. Radial variation near the transonic wind base of the velocity v and the line-ensemble-averaged source function s_α (normalized to the optically thin value). The dashed curve applies at the CAK initial condition, while the solid curve gives results for at time 100 ksec later in an EISF simulation. b. Corresponding variations of this scaled source function s_α vs. wind velocity.

However, in the SSF model with scattering, there now develops in this region a *positive* diffuse force, resulting from the strong steepening of the velocity gradient near the sonic point, which makes $b_- > b_+$ and so through eqn. (18) gives a positive diffuse force. Quite remarkably when added to the direct term, this gives a total force that follows very closely the CAK/Sobolev force throughout the subsonic and transonic region. This explains why the (drag-effect stabilized) base outflow in SSF simulations follows very closely the CAK solution, and why co-moving-frame models [30] of line-driven winds also match well the (finite-disk-corrected) CAK model. In effect, the addition of the SSF diffuse force corrects for the non-Sobolev error in the pure-absorption force, making the total force accurate to a higher order in the parameter l_{Sob}/H. This suggests that the validity of a CAK/Sobolev approach, for which the diffuse force is normally assumed to vanish and thus play no role, actually depends crucially on the scattering nature of line-transport for proper wind initiation near the transonic base!

But the situation is further complicated by the EISF results, which instead give a *negative* diffuse force in the subsonic region. This stems from the strong "dip" in the EISF source function near and below the sonic point, as shown in the right panels of figure 5. Much like the SSF diffuse force, this dip results from the velocity gradient steepening and associated asymmetries in the escape probabilities near the sonic point. The lower subsonic gradient implies a lower b_+ to shift core radiation into line resonance, while the large outward gradient leads to a higher b_- that enhances the escape from the resonance zone. This lowers the mean intensity, and by eqn. (20), the source function. But then the strong outward increase in mean intensity from this dip implies a strong *inward diffusion* of line-flux, giving rise to the inward diffuse line-force. The net result is to weaken the total force even below its pure-absorption value, yielding then a reduction in the mass flux that can be driven through the sonic point.

While the EISF method does not represent a fully consistent radiative transfer solution, such source function dips have been seen in model atmospheres with full NLTE solutions of the line transfer [37]. It is unclear why the effect was not seen in the co-moving-frame calculations of [30], but one possibility is that this analysis was for a relatively dense supergiant wind, for which coupling to the continuum and thermalization effects might help keep the line source function elevated, and smooth, in the sonic region. If true, this would imply that the SSF method and results might be quite appropriate for dense winds from OB supergiants. However, for late O and cooler main sequence stay, the effects of a source-function dip could be significant, perhaps even playing a role in their "weak wind" problem [33]. Such effects should also be considered in the context of recent renewed interest in the role of atmospheric microturbulence on the wind mass loss rate [14].

In conclusion, it seems that some 40 years after the initial work on line-driven stellar winds, both wind instability and wind initiation remain key issues for understanding their radiation hydrodynamics. To end with a personal note, I first learned about stellar winds as a graduate student in Dimitri Mihalas' Spring 1977 course on "Stellar Atmospheres" at the University of Colorado, and indeed even wrote my term paper on the subject. In grading that paper, Dimitri wrote on the cover page, "Interesting paper; I hope you will follow it up with some future research". In perusing this volume of papers from the conference in honor of his 70th birthday, perhaps he will be amused to see that at least one ex-student has endeavored to take his advice.

ACKNOWLEDGMENTS

This work was carried out with partial support by NASA grant LTSA/NNG05GC36G, and by NSF grant AST-0507581.

REFERENCES

1. Abbott, D. C. 1980, ApJ, 242, 1183.
2. Abbott, D.C. 1982, ApJ, 259, 282.
3. Castor, J., Abbott, D., & Klein, R. 1975, ApJ 195, 157 (CAK).
4. Davidson, K., & Humphreys, R.M. 1997, Ann Rev Astr Astrophys 35, 1

5. Dessart, L. and Owocki, S.P. 2003, ApJ 406, 1.
6. Eddington, A.S. 1926, *The Internal Constitution of the Stars*, Chapter 6.
7. Feldmeier, A. 1995, A&A, 299, 523
8. Feldmeier, A., Puls, J., and Pauldrach, A. 1997, A&A 322, 878.
9. Figer, D. F. 2005, Nature 434, 192
10. Friend, D. B. & Abbott, D. C. 1986, ApJ, 311, 701
11. Gayley, K. 1995, ApJ 454, 410
12. Kudritzki, R.-P. Lennon, D. J., & Puls, J. 2009 in *Science with the VLT*, J. R. Walsh & I. J. Danziger, eds., 1995, p. 246
13. Lucy, L. B. 1984, ApJ, 284, 351
14. Lucy, L. B. 2007, A&A, 474, 701
15. Lucy, L. B., & Solomon, P. 1970, ApJ 159, 879
16. MacGregor, K. B., Hartmann, L., & Raymond, J. C. 1979, ApJ, 231, 514
17. Oskinova, L. M., Hamann, W.-R., & Feldmeier, A. 2007, A&A 476, 1331
18. Owocki, S. P. 1991, NATO ASIC Proc. 341: Stellar Atmospheres - Beyond Classical Models, 235
19. Owocki, S. 2004, EAS Publications Series, 13, 163
20. Owocki, S. P., Castor, J. I., & Rybicki, G. B. 1988, ApJ 335, 914
21. Owocki, S. P., & Cohen, D. H. 2006, ApJ 648, 565
22. Owocki, S., Gayley, K., & Shaviv, N. 2004, ApJ 558, 802
23. Owocki, S. P., & Puls, J. 1996, ApJ 462, 894
24. Owocki, S. P., & Puls, J. 1999, ApJ 510, 355
25. Owocki, S.P. and Rybicki, G.B. 1984, ApJ 284, 337
26. Owocki, S.P. and Rybicki, G.B. 1985, ApJ 299, 265
27. Owocki, S. P., & ud-Doula, A. 2004, ApJ 600, 1004
28. Owocki, S., & van Marle, A. J. 2008, IAU Symposium, 250, 71
29. Pauldrach, A. 1987, A&A 183, 295
30. Pauldrach, A., Puls, J., Kudritzki, R.P. 1986, A&A 164, 86
31. Poe, C. H., Owocki, S. P., & Castor, J. I. 1990, ApJ 358, 199
32. Puls, J. 1994, Habilitation thesis, Univ. Munich
33. Puls, J., Sundqvist, J. O., Najarro, F., and Hanson, M. M. 2009, these proceedings.
34. Runacres, M. C., & Owocki, S. P. 2002, A&A 381, 1015
35. Runacres, M. C., & Owocki, S. P. 2005, A&A 429, 323
36. Rybicki, G.B., Owocki, S.P., and Castor, J.I. 1990, ApJ 349, 274
37. Sellmaier, F., Puls, J., Kudritzki, R. P., Gabler, A., Gabler, R., & Voels, S. A. 1993 A&A 273, 533
38. Sobolev, V. V. 1960, *Moving Envelopes of Stars* (Cambridge: Harvard University Press).
39. Vishniac, E.T. 1994, ApJ 428, 186.